Cation ordering in magnesioferrite, MgFe$_2$O$_4$, to 982 °C using in situ synchrotron X-ray powder diffraction

SYTLE M. ANTAO,[1,*] ISHMAEL HASSAN,[2] AND JOHN B. PARISE[1]

[1]Mineral Physics Institute and Department of Geosciences, State University of New York, Stony Brook, New York 11794-2100, U.S.A.
[2]Department of Chemistry, University of the West Indies, Mona, Kingston 7, Jamaica

ABSTRACT

Magnesioferrite spinel, MgFe$_2$O$_4$, was synthesized at 900 °C from equimolar amounts of reagent-grade oxides, MgO and Fe$_2$O$_3$, and quenched in air. The structural behavior of magnesioferrite was determined from in situ synchrotron X-ray powder-diffraction data [$\lambda = 0.92225(4)$ Å] at room pressure and temperatures from 28 to 982 °C on heating and cooling. The a unit-cell parameter increases linearly on heating, but deviates to give a discontinuity at 581 °C. Above 581 °C and on cooling from 982 °C, the a parameter varies linearly. The a parameter at 28 °C before heating [8.39704(5) Å] and after cooling to 47 °C [8.39514(4) Å] is different because the cation order frozen in the structure is not the same. Cation order, analyzed in terms of the inversion parameter, x, {^{iv}[Mg$_{1-x}$Fe$_x$]^{vi}[Mg$_{x/2}$Fe$_{1-x/2}$]$_2$O$_4$}, and the order parameter, $Q = 1 - (3/2)\,x$, show no change on heating until the temperature is high enough to cause exchange of Mg^{2+} and Fe^{3+} cations between the octahedral and tetrahedral sites. This activation barrier is overcome at 581 °C, where the sample achieves the maximum ordered state on heating [$x_{max} = 0.867(4)$] and begins to move toward equilibrium. This relaxation is toward a more ordered configuration and is a kinetically controlled process. Above 581 °C, the cations continuously disorder along the equilibrium pathway to the maximum temperature studied [$T_{max} = 982$ °C, $x = 0.769(3)$] and reverse along the equilibrium pathway on cooling. At T_B, the maximum equilibrium order is frozen in, and maintained to room temperature, where $x_{max} = 0.895(4)$. O'Neill-Navrotsky, Landau, and Ginzburg-Landau models give good descriptions of the ordering process in MgFe$_2$O$_4$. Simultaneous differential scanning calorimetry (DSC) and thermogravimetry (TG) data were obtained using a Netzsch STA 449C simultaneous TG-DSC instrument. The DSC curve for MgFe$_2$O$_4$ contains an irreversible exothermic peak at about 550 °C = T_{relax} in the first heating experiment, and the energy change associated with this peak is –162 J/g (= –32 KJ/mol), and corresponds to cation relaxation. From Rietveld refinements, $T_{relax} \approx 581$ °C. The $T_{Curie} \approx 360$ °C was obtained from TG experiments carried out in a magnetic field.

INTRODUCTION

Numerous studies have been carried out on spinels because of their chemical and structural simplicity, their geological importance, and their use as geothermometers, geobarometers, and geospeedometers (e.g., O'Neill and Wall 1987; Sack 1982). In situ measurements are more realistic than measurements on quenched samples to study the structural behavior of minerals because the cation distribution, especially at high temperatures, is unquenchable (O'Neill et al. 1992). This study aims to solve the quench problem, and to determine and thermodynamically model the cation order to about 1000 °C for magnesioferrite, ideally MgFe$_2$O$_4$.

The spinel structure consists of tetrahedrally coordinated cations at 8a (1/8, 1/8, 1/8), octahedrally coordinated cations at 16d (1/2, 1/2, 1/2), and O atoms on the body diagonals of a cube at 32e (u, u, u), where u is approximately 1/4 in space group $Fd\bar{3}m$ (Fig. 1). In a perfectly ordered cubic structure, there are only two structural variables (except displacement parameters): the a unit-cell parameter and the O atom positional parameter u.

Cubic spinels have the general formula AB$_2$O$_4$. The A and B cation charges may be either +2 and +3 (e.g., magnesioferrite, MgFe$_2$O$_4$), or +4 and +2 (e.g., qandilite, TiMg$_2$O$_4$). In "normal" spinels, the A cation occupies the tetrahedral site and the B cation occupies the octahedral site. In fully "inverse" spinels, the tetrahedral (IV) site contains only B cations and the octahedral (VI) site contains an equal number of A and B cations, so the octahedral site is disordered. Any intermediate spinel may be expressed as a mix of the normal and inverse end-members, with general formula: ^{IV}[A$_{1-x}$B$_x$]^{VI}[A$_{x/2}$B$_{1-x/2}$]$_2$O$_4$, where the variable x is referred to as the "inversion parameter". This x is the fraction of B cations at the tetrahedral site. In normal spinels $x = 0$, and in inverse spinels $x = 1$. A value of $x = 2/3$ corresponds to a completely random distribution of A and B cations. Alternatively, an order parameter, Q, is used to express the degree of order (see Harrison et al. 1998), and varies from $Q = 1$ for a completely ordered normal spinel, to $Q = 0$ (where $x = 2/3$) for a random arrangement of cations, to $Q = -0.5$ in inverse spinel. The relationship between Q and x is: $Q = 1 - (3/2)\,x$. MgFe$_2$O$_4$ is partly inverse and partly normal and is, therefore, one of the most interesting ferrite spinels (Paladino 1960).

* E-mail: sytle.antao@stonybrook.edu
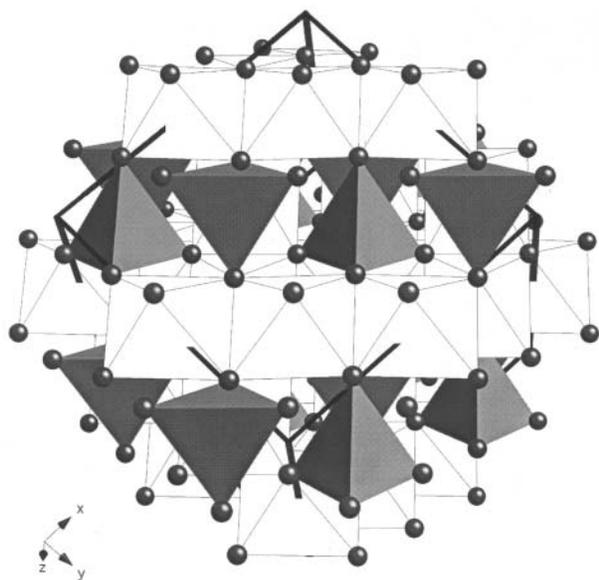
FIGURE 1. Projection of the structure of MgFe$_2$O$_4$ at 28 °C. The tetrahedral and octahedral cation sites are shown in grey and white, respectively, and the O atoms as small circles. A unit cell is outlined.

Spinels tend to be completely disordered as the temperature is increased (e.g., O'Neill et al. 1992; Faller and Birchenall 1970; Mozzi and Palladino 1963). The order-disorder process in spinels is termed "non-convergent" because there is no symmetry change upon disordering. A completely random distribution would occur at infinite temperature, and is approached asymptotically with increasing temperature. However, some spinels melt before disorder is complete (Faller and Birchenall 1970). Interest in spinels arises from the ability of two different cations to disorder over two separate cation sites. This disorder phenomenon is called substitutional disorder, and is exhibited by numerous rock-forming minerals (e.g., Hazen and Navrotsky 1996).

Samples of MgFe$_2$O$_4$ used in previous studies have different stoichiometries, therefore, the results may not be comparable (e.g., Bacon and Roberts 1953; Mozzi and Paladino 1963; Allen 1966; Walters and Wirtz 1971; Faller and Birchenall 1970; Nell et al. 1989; O'Neill et al. 1992; Harrison and Putnis 1999). Departure from stoichiometry in MgFe$_2$O$_4$ results from: (1) substitution of Fe^{2+} for Mg^{2+} causing solid solution toward Fe$_3$O$_4$; (2) solid solution toward γ-Fe$_2$O$_3$ (maghemite); and (3) excess MgO (O'Neill et al. 1992). To synthesize stoichiometric MgFe$_2$O$_4$, the temperature should be less than 1000 °C, and the presence of excess MgO avoids the solid-solution problem. The synthesis temperature in this study was 900 °C for magnesioferrite. An X-ray diffraction (XRD) pattern for our sample showed that it was crystalline, although O'Neill et al. (1992) stated that a synthesis temperature below 950 °C would give a non-crystalline product.

Studies of magnesioferrite quenched from various temperatures are available (e.g., Harrison and Putnis 1999; O'Neill et al. 1992; Allen 1966; Walters and Wirtz 1971; Faller and Birchenall 1970). Quenched samples may not be representative of the cation order at the particular annealing temperature because the quenching rate may not be rapid

enough to preserve the cation distribution (O'Neill et al. 1992). Therefore, in situ measurements at high temperatures are more reliable than measurements on quenched samples.

This study determines the cation order in magnesioferrite, MgFe$_2$O$_4$, at room pressure and from 28 to 982 °C on heating and cooling. These results are used to compare the thermodynamic models for cation ordering; namely the O'Neill and Navrotsky (1983), Landau (Carpenter et al. 1994; Carpenter and Salje 1994), and the Ginzburg-Landau (Carpenter and Salje 1989; and Salje 1988) models. Some recent magnesioferrite data are also included for comparison (Levy et al. 2004).

EXPERIMENTAL METHODS

Synthesis

The brown MgFe$_2$O$_4$ sample was synthesized from equimolar amounts of dried reagent-grade oxides: MgO (slightly excess) and Fe$_2$O$_3$. The oxides were ground together under ethanol in an automated agate mortar for 2 hours. The mixture was dried and sintered at 900 °C for ten days in an evacuated SiO$_2$ glass capsule lined with Ag foil. MgFe$_2$O$_4$ was quenched from 900 °C by gently removing the SiO$_2$ glass capsule from the oven and placing it on a brick to cool in air to room temperature. The sintered sample was finely crushed in an agate mortar and pestle under ethanol for the experimental work. Phase identity and purity were established by powder X-ray diffraction using an automated Scintag PAD-X diffractometer operating in the θ-θ mode [Cu(Kα) radiation: Kα$_1$ = 1.540562 and Kα$_2$ = 1.544390 Å; operating at 45 kV and 35 mA; step time = 2 s and step size = 0.2 °, using the step scan mode; 2-θ range = 5 to 120 °] and optical examination. Previous studies of magnesioferrite involved synthesis in platinum capsules (e.g., O'Neill et al. 1992), but platinum contact was avoided in this study because it alloys with iron (Merrill and Wyllie 1973).

The chemical analysis for magnesioferrite (using a small amount of uncrushed sample encapsulated in epoxy resin) was done using a Cameca Camebax electron microprobe (EMP) with the operating program MBX (copyright by Carl Henderson, University of Michigan), and data correction using Cameca's PAP program. The analytical conditions were 15 kV and 9.6 nA beam current. Natural minerals were used as standards: forsterite (MgKα) and hematite (FeKα). The chemical formula, Mg$_{1.0003}$Fe$_{1.9998}$O$_4$, was arrived at by averaging 15 analyses obtained from different grains. The chemical formula obtained shows that it is stoichiometric.

High-temperature synchrotron X-ray powder diffraction

In situ high-temperature synchrotron X-ray powder-diffraction experiments were performed at beam-line X7B [λ = 0.92225(4) Å] of the National Synchrotron Light Source at Brookhaven National Laboratory. The sample was loaded in a quartz capillary (diameter = 0.5 mm and open to air at one end). Elevated temperatures were obtained using a horseshoe-shaped heater and controlled using a thermocouple element near the capillary. The sample was oscillated during the experiment over an angle of 30°. Diffraction patterns were collected at room pressure and from 28 to 982 °C on heating, and on cooling from 982 to 28 °C, in regular intervals of about 19 °C. The sample was heated or cooled at a rate of about 9.5 °C/min. Data were collected to a maximum 2θ of about 50° [(sinθ/λ) < 0.46 Å^{-1}]. An imaging plate (IP) detector (Mar345, 2300 × 2300 pixels) mounted perpendicular to the beam path was used to collect Debye-Scherrer rings with an exposure time of 30 s. In a separate experiment, a LaB$_6$ standard was used to determine the sample-to-detector distance, tilt angle, wavelength, and tilting angle of the IP. Diffraction traces recorded by the IP were integrated using the Fit2d program (Hammersley 1996).

Thermal analyses

Simultaneous differential scanning calorimetry (DSC) and thermogravimetry (TG) data were obtained using a Netzsch STA 449C TG-DSC instrument. About 15 mg of sample was loaded into an Al$_2$O$_3$ crucible for the first experiment. Data were collected in a static air environment at a heating rate of 10 °C/min from 25 to 1400 °C, and at the same rate on cooling down to 25 °C. In a second heating experiment, about 8 mg of sample was used for three consecutive heating and cooling cycles from 100 to 800 °C in a magnetic field, which was obtained by placing two magnets outside the furnace in the vicinity of the sample position. The TG curve was corrected for buoyancy effect, and the DSC curve was corrected for baseline effect. Corrections for buoyancy and baseline effects were obtained in a blank experiment using empty crucibles that were later used to contain the sample

in a second experiment; both experiments were made under identical conditions. The data were analyzed using the software programs provided with the instrument. The TG curve shows the change in weight as a function of temperature. The DSC curve shows the change in energy as a function of temperature. The DDSC curve is the derivative of the DSC curve.

RESULTS AND DISCUSSION

Rietveld structure refinements

Forty-five diffraction patterns collected at regular temperature intervals were selected for treatment with the Rietveld method using the GSAS and EXPGUI programs (Larson and Von Dreele 2000; Toby 2001). For the room-temperature structure, the starting atomic coordinate, cell parameter, isotropic displacement parameters, and space group, $Fd\bar{3}m$ [origin $(\bar{3}m)$ at 1/8, 1/8, 1/8 from $(\bar{4}3m)$], were from O'Neill et al. (1992). Initially, the 8a and 16d cation sites and 32e O atom sites were constrained to be fully occupied, i.e., the site occupancies were fixed to the idealized stoichiometric chemical formula, MgFe₂O₄. The refined structural parameters were then used as input for the next higher-temperature structure.

The background was modeled using a Chebyschev polynomial function of the first kind. A total of 32 coefficients were needed to model the background "hump" of the quartz capillary used to hold the sample. The reflection-peak profiles were fitted using an asymmetry correction and three coefficients (asym, GW, GV, and LY). The zero-shift was set to zero at all temperatures, as the instrument was calibrated with a LaB₆ standard. The beam intensity was gradually decreasing as the experiment progressed, as judged by the counts for the strongest (311) reflection at 20.9° 2θ. At the start of the experiment, the (311) reflection had about 50 000 counts, but at the end it had about 16 000 counts. Because of the decreasing intensity, the peak-to-background ratio deteriorated, especially for the 111 reflection, which is located on the background "hump" of the quartz capillary. However, as the background was fitted quite well, the data were still good, and the decreasing χ² is a result of the low peak-to-background ratio (see Table 1). A full-matrix least-squares refinement,

TABLE 1. Magnesioferrite: Rietveld refinement* and structure data (top set: heating, bottom set: cooling)

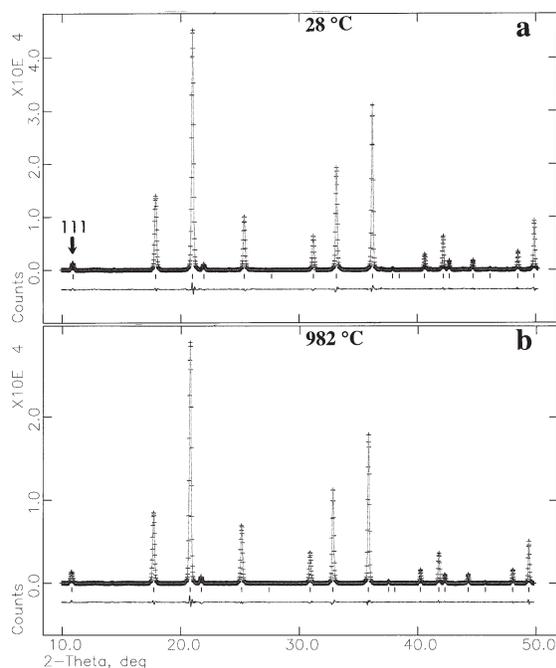| T (°C)	a (Å)	x	u	$R_p \times 100$	$R_{wp} \times 102$	ExpR_{wp} ×102	$R_F^2 \times 102$	χ^2	$U_{(O)}$ × 102(Å²)	$U_{(tet)}$ × 102(Å²)	$U_{(oct)}$ × 102(Å²)	$I_{tet} - O$(Å) – O(Å)	$I_{oct} - O$ (Å) – O (Å)
28	8.39704(5)	0.841(4)	0.2548(2)	0.99	1.63	1.35	1.13	1.497	0.52(5)	0.11(4)	0.22(4)	1.888(3)	2.060(1)
47	8.39769(5)	0.840(4)	0.2550(2)	0.97	1.64	1.35	1.34	1.506	0.53(5)	0.20(4)	0.32(4)	1.891(3)	2.058(1)
105	8.40360(5)	0.839(4)	0.2548(2)	0.97	1.59	1.34	1.18	1.435	0.66(5)	0.25(4)	0.40(4)	1.890(3)	2.061(1)
143	8.40578(5)	0.839(4)	0.2549(2)	0.95	1.58	1.34	1.33	1.415	0.70(5)	0.30(4)	0.47(4)	1.891(3)	2.061(1)
200	8.41019(5)	0.839(4)	0.2549(2)	0.94	1.58	1.36	1.30	1.387	0.74(5)	0.35(4)	0.54(4)	1.892(3)	2.062(1)
257	8.41634(5)	0.839(4)	0.2550(2)	0.93	1.57	1.37	1.29	1.345	0.82(8)	0.47(4)	0.66(4)	1.894(3)	2.063(1)
295	8.42079(5)	0.836(4)	0.2550(2)	0.90	1.51	1.37	1.43	1.237	0.89(5)	0.45(4)	0.70(4)	1.893(3)	2.066(1)
353	8.42712(5)	0.838(4)	0.2549(2)	0.91	1.51	1.39	1.42	1.215	0.97(5)	0.63(4)	0.85(4)	1.897(2)	2.066(1)
410	8.43043(5)	0.837(4)	0.2547(2)	0.87	1.47	1.39	1.37	1.144	1.05(5)	0.57(4)	0.82(4)	1.894(3)	2.069(1)
448	8.43439(5)	0.839(4)	0.2546(2)	0.89	1.49	1.42	1.29	1.127	1.11(5)	0.60(4)	0.89(4)	1.893(3)	2.071(1)
505	8.43699(5)	0.850(4)	0.2544(2)	0.83	1.40	1.43	1.31	0.981	1.16(5)	0.62(4)	0.92(4)	1.891(2)	2.073(1)
543	8.43829(5)	0.861(4)	0.2544(2)	0.83	1.40	1.44	1.32	0.961	1.22(5)	0.66(4)	0.98(4)	1.891(3)	2.073(1)
562	8.44178(5)	0.863(4)	0.2542(2)	0.85	1.41	1.45	1.18	0.955	1.29(5)	0.71(4)	1.03(4)	1.889(3)	2.076(1)
581	8.44082(4)	0.867(4)	0.2542(2)	0.84	1.40	1.46	1.22	0.939	1.27(5)	0.69(4)	0.99(4)	1.889(3)	2.075(1)
601	8.44366(5)	0.859(4)	0.2542(2)	0.82	1.42	1.46	1.27	0.966	1.32(5)	0.71(4)	1.03(4)	1.890(3)	2.076(1)
658	8.44737(5)	0.849(4)	0.2541(2)	0.82	1.39	1.47	1.18	0.912	1.39(5)	0.76(4)	1.06(4)	1.890(3)	2.077(1)
696	8.45225(5)	0.834(4)	0.2544(2)	0.91	1.51	1.48	2.11	1.050	1.56(5)	0.91(4)	1.14(4)	1.891(3)	2.078(1)
753	8.45830(5)	0.818(4)	0.2542(2)	0.80	1.39	1.50	1.03	0.875	1.60(5)	0.91(4)	1.18(4)	1.893(2)	2.080(1)
791	8.46018(5)	0.814(4)	0.2542(2)	0.83	1.39	1.51	1.18	0.865	1.66(5)	0.95(4)	1.20(4)	1.893(2)	2.081(1)
848	8.46608(4)	0.797(3)	0.2541(2)	0.78	1.31	1.54	1.01	0.748	1.74(5)	0.98(4)	1.24(4)	1.893(2)	2.082(1)
906	8.47175(4)	0.780(3)	0.2542(2)	0.75	1.28	1.56	1.07	0.689	1.85(5)	1.05(4)	1.33(4)	1.896(2)	2.083(1)
944	8.47516(4)	0.773(3)	0.2543(2)	0.76	1.28	1.55	1.09	0.699	1.90(5)	1.10(4)	1.36(4)	1.897(2)	2.083(1)
982	8.47670(4)	0.769(3)	0.2543(2)	0.76	1.27	1.57	1.07	0.676	1.90(5)	1.10(4)	1.38(4)	1.898(2)	2.083(1)
963	8.47405(5)	0.772(4)	0.2538(2)	0.84	1.43	1.57	1.19	0.847	1.74(5)	0.77(4)	1.09(4)	1.891(3)	2.087(1)
944	8.47392(4)	0.774(3)	0.2542(2)	0.76	1.25	1.58	1.13	0.636	1.87(5)	1.07(4)	1.33(4)	1.896(2)	2.084(1)
906	8.47029(4)	0.787(3)	0.2543(2)	0.77	1.27	1.59	1.12	0.645	1.82(5)	1.05(4)	1.33(4)	1.896(2)	2.082(1)
848	8.46438(4)	0.803(3)	0.2543(2)	0.75	1.25	1.61	1.10	0.608	1.66(5)	0.92(4)	1.19(4)	1.895(2)	2.081(1)
791	8.46211(4)	0.811(4)	0.2540(2)	0.82	1.27	1.63	0.78	0.618	1.66(5)	0.87(4)	1.11(4)	1.891(2)	2.082(1)
753	8.45708(4)	0.826(4)	0.2543(2)	0.75	1.25	1.62	1.19	0.610	1.51(5)	0.82(4)	1.08(4)	1.894(2)	2.079(1)
715	8.45245(4)	0.825(4)	0.2543(2)	0.66	1.14	1.62	1.08	0.503	1.67(6)	0.63(4)	1.12(4)	1.892(2)	2.078(1)
696	8.45180(4)	0.843(4)	0.2543(2)	0.72	1.16	1.63	1.10	0.517	1.35(5)	0.73(4)	0.99(4)	1.893(2)	2.077(1)
658	8.44813(4)	0.857(4)	0.2543(2)	0.74	1.15	1.62	1.03	0.518	1.30(5)	0.70(4)	0.94(4)	1.891(2)	2.077(1)
601	8.44122(4)	0.875(4)	0.2543(2)	0.69	1.08	1.64	1.11	0.449	1.12(5)	0.60(4)	0.85(4)	1.891(2)	2.074(1)
562	8.43831(4)	0.877(4)	0.2546(2)	0.58	1.01	1.64	1.27	0.388	1.05(5)	0.52(4)	0.85(4)	1.894(2)	2.072(1)
543	8.43712(4)	0.881(4)	0.2543(2)	0.68	1.05	1.64	1.22	0.420	1.03(5)	0.51(4)	0.80(4)	1.890(2)	2.073(1)
505	8.43375(4)	0.888(4)	0.2543(2)	0.75	1.09	1.64	1.12	0.453	0.97(5)	0.50(4)	0.76(5)	1.889(3)	2.073(1)
448	8.42961(4)	0.888(4)	0.2547(2)	0.65	1.00	1.66	1.40	0.371	0.84(5)	0.45(4)	0.72(4)	1.894(2)	2.069(1)
410	8.42558(4)	0.890(4)	0.2546(2)	0.67	1.00	1.68	1.29	0.357	0.79(5)	0.38(4)	0.62(4)	1.891(2)	2.069(1)
353	8.42080(4)	0.890(4)	0.2546(2)	0.66	0.99	1.71	1.27	0.344	0.71(5)	0.28(4)	0.54(4)	1.890(2)	2.067(1)
295	8.41415(4)	0.893(4)	0.2547(2)	0.71	1.01	1.73	1.31	0.349	0.62(5)	0.26(4)	0.43(4)	1.891(2)	2.065(1)
257	8.41259(4)	0.889(4)	0.2548(2)	0.63	0.96	1.74	1.34	0.312	0.53(5)	0.12(4)	0.35(4)	1.891(2)	2.064(1)
200	8.40607(4)	0.892(4)	0.2546(2)	0.67	0.99	1.77	1.40	0.316	0.49(5)	0.06(4)	0.22(4)	1.888(2)	2.063(1)
143	8.40084(4)	0.894(4)	0.2545(2)	0.66	0.97	1.78	1.35	0.306	0.56(5)	0.09(4)	0.24(4)	1.885(2)	2.063(1)
105	8.39837(4)	0.896(4)	0.2546(2)	0.65	0.98	1.80	1.39	0.303	0.51(5)	0.06(4)	0.16(4)	1.886(2)	2.062(1)
47	8.39514(4)	0.895(4)	0.2546(2)	0.67	0.96	1.83	1.37	0.280	0.48(5)	0.03(4)	0.16(4)	1.885(2)	2.062(1)

*R_p = pattern R factor = $\{\Sigma[|(I_o - I_c)|]/\Sigma I_o\}$; R_{wp} = weighted pattern R factor = $\{\Sigma[w(I_o - I_c)^2]/\Sigma[wI_o^2]\}^{1/2}$, where I_o = observed intensity, I_c = calculated intensity, and w = $1/I_o$; R_p and R_{wp} are the fitted values obtained without background subtraction. Exp R_{wp} = expected value of R_{wp} = R_e. R_F^2 = R-structure factor based on observed and calculated structure amplitudes = $\{\Sigma[(F_o^{1/2} - F_c^{1/2})|]/\Sigma F_o^{1/2}$; $\chi^2 = [R_{wp}/R_e]$; where $R_e = [(N - P)/(\Sigma wI_o^2)]^{1/2}$, where N is the no. of observations (data points; ≈ 2120) and P is the no. of variables (= 43).

varying a scale factor, cell parameter, atomic coordinate, and isotropic displacement parameters, converged quickly. The cations at equivalent sites were constrained to have equal isotropic displacement parameters (e.g., Mg^{2+} and Fe^{3+} cations at the 8a site). In Rietveld structure refinements, it is common to use isotropic displacement parameters, and to constrain similar atoms to have equal isotropic displacement parameters (e.g., Harrison et al. 1998; Redfern et al. 1999). The cation site occupancy factor, x, was introduced as a variable and refined. Toward the end of the refinement, all parameters (32 background terms, 4 profile parameters, cell, scale factor, and 5 structural parameters; total variables, $P = 43$) were allowed to vary, and the refinement proceeded to convergence. The number of observed reflections in a typical XRD pattern is 21, and the number of observations (data points) is about 2120. Example of synchrotron X-ray powder diffraction patterns are shown in Figure 2. The structural parameters and the Rietveld refinement statistics at various temperatures are listed in Table 1.

Structure of magnesioferrite

The general structural features of MgFe$_2$O$_4$ have been described (Fig. 1). Using synchrotron data, at 28 °C, a = 8.39704(5) Å, the inversion parameter, x, is 0.841(4), the O atom positional parameter, u = 0.2548(2), is close to the ideal value of 1/4, and the interatomic distances to the tetrahedral ($l_{\text{tet-O}}$) and octahedral ($l_{\text{oct-O}}$) sites are 1.888(3) and 2.060(1) Å, respectively (Table 1).

The following results were obtained from a GSAS refinement of the Scintag data: χ^2_c = 1.374, R_F^2 = 0.0605, a = 8.39705(5) Å, x =0.840(5), u = 0.2568(3), $l_{\text{tet-O}}$ = 1.918(4) Å and $l_{\text{oct-O}}$ = 2.043(2) Å.

Cell parameter

The a value for stoichiometric MgFe$_2$O$_4$ ranges between 8.38–8.40 Å (O'Neill et al. 1992). In this study, a = 8.39704(5) Å at 28 °C (Table 1). The cell parameter obtained from the Scintag data was 8.39705(9) Å, which also falls within the range reported for stoichiometric MgFe$_2$O$_4$. In addition, refinement of the cation site occupancies indicated that our sample is stoichiometric.

The cell parameter depends on the amount of disorder frozen in the structure after quenching from the synthesis temperature, so the quenching rate is important. In this study, the sample was removed from the oven and placed on a brick to cool to 25 °C. Harrison and Putnis (1999) quenched their sample by dropping it into water and obtained a = 8.399(2) Å, a slightly larger cell. O'Neill et al. (1992) also quenched their samples in water.

The a parameter of MgFe$_2$O$_4$ increases linearly on heating, but it gives a discontinuity at about 581 °C (Fig. 3). Above 581 °C, a is also linear. This discontinuity coincides with the maximum cation order observed on heating, which causes a decrease in the cell volume. Cooling from 982 °C, the a parameter decreases linearly. The path on cooling is different from that on heating, especially at lower temperatures. The a parameter before heating [8.39704(5) Å at 28 °C] and after cooling [8.39514(4) Å at 47 °C] is different, because of the different cation order frozen in the structure. The sample is more ordered after cooling, which results in a smaller cell. Therefore, a can be a sensitive indicator of cation distribution (O'Neill et al. 1992). Large volume corresponds to a more disordered cation distribution. However, the volume change with cation distribution is better determined from quenched samples, because the volume change is not obscured by

FIGURE 2. Synchrotron X-ray powder-diffraction pattern for MgFe$_2$O$_4$ at 28 and 982 °C, together with the calculated (continuous line) and observed (crosses) profiles. The difference curve ($I_{\text{obs}} - I_{\text{calc}}$) is shown at the bottom. The short vertical lines indicate allowed reflection positions. Peak 111 is higher at 982 °C compared to 28 °C, indicating more disorder at higher temperatures.
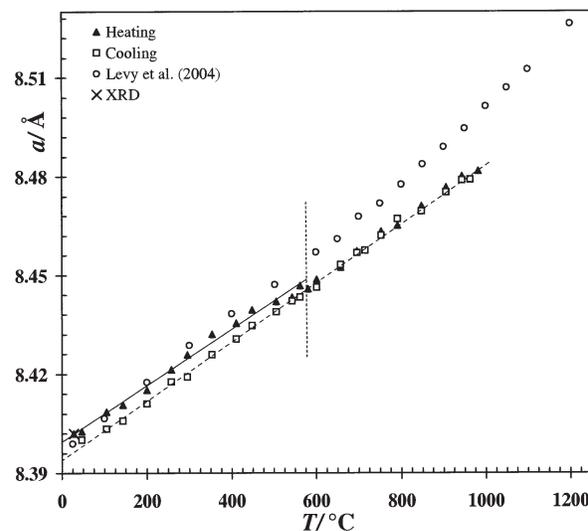

FIGURE 3. The a unit-cell parameter of MgFe$_2$O$_4$: a increases linearly on heating, but it deviates at 581 °C, as indicated by the vertical dashed line. Above 581 °C and cooling from 982 °C, a varies linearly. Error bars are smaller than the symbols.

the concurrent thermal-expansion effect (O'Neill et al. 2003).

The cell parameters of O'Neill et al. (1992) are different from those obtained in this study because they used samples quenched from various temperatures to preserve cation distributions, but the cell dimensions with the effects of thermal expansion could not be quenched. No break in the linearity of the a parameter was observed by O'Neill et al. (1992), because their cation distributions were at equilibrium and varied smoothly with temperature. However, we observed equilibrium and non-equilibrium cation distributions.

Order parameters

Cation order in MgFe₂O₄ is analyzed in terms of the inversion parameter, x, indicated by the formula, $^{IV}[Mg_{1-x}Fe_x]^{VI}[Mg_{x/2}Fe_{1-x/2}]_2O_4$, and the order parameter, $Q = 1 - (3/2) x$. Initially, $x = 0.841(4)$ at 28 °C for MgFe₂O₄ and corresponds to x quenched from synthesis at 900 °C. However, this is not the same x as that observed in situ at 906 °C [0.780(3) on heating, and 0.787(3) on cooling; Table 1]. This indicates that the quenching rate was not rapid enough to preserve the cation distribution at 900 °C, which is expected as the sample was removed from the oven and left to cool in air to 25 °C, because we did not try to quench in the cation order at 900 °C. This quenched-in cation distribution differs from the equilibrium cation distribution because of the fast kinetics of ordering, which allows rapid redistribution during quenching (e.g., Redfern et al. 1996).

The cation order quenched from the synthesis temperature is disordered relative to the equilibrium distribution. Therefore, there is a driving force for the system to order. On heating, there is no change in x until the temperature is high enough to cause exchange of Mg^{2+} and Fe^{3+} cations between the octahedral and tetrahedral sites because of the slow kinetics of ordering within this temperature range (Fig. 4). This activation barrier is overcome at about 581 °C, where MgFe₂O₄ achieves maximum cation order [$x = 0.867(4)$] on heating and begins to move toward equilibrium. The rapid approach toward equilibrium on heating is referred to as "relaxation" of the cation distribution and is a kinetically controlled process (Harrison et al. 1998; Redfern et al. 1999). Heating beyond 581 °C causes the cations to disorder along the equilibrium pathway to the maximum temperature studied [$T_{max} = 982$ °C, $x = 0.769(3)$]. At 658 °C, $x_{658 °C} = 0.849(4)$ and at 696 °C, $x_{696 °C} = 0.834(4)$, so the calculated value at $x_{677 °C} = 0.842(4)$ is similar to $x_{28 °C} = 0.841(4)$. This suggests that the blocking temperature for the Mg^{2+}-Fe^{3+} cation exchange during quenching from the synthesis temperature was close to about 677 °C (see Henderson et al. 1996).

On cooling from 982 °C, the cation ordering reverses along the equilibrium pathway to the blocking temperature, $T_B \approx 543$ °C, which occurs at a lower temperature than during quenching after synthesis (677 °C) because of the slower cooling rate (Fig. 4). On cooling below T_B, the maximum equilibrium order at T_B is frozen in the structure [$x_{max} = 0.895(4)$].

Data from O'Neill et al. (1992) are different from those obtained in this study (Fig. 4). The disorder they observed (and quenched) at higher temperatures is greater than that observed in situ in this study [e.g., at 944 °C, we obtained 0.773(3) and 0.774(3), whereas O'Neill et al. (1992) obtained 0.749(4) at 950 °C; Fig. 4]. This is probably because of the difference in
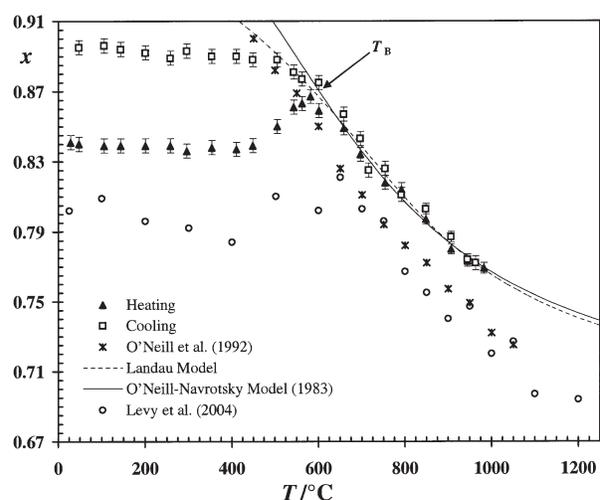
FIGURE 4. The inversion parameter, x, for MgFe₂O₄. On heating, x is constant to 448 °C, and at 581 °C the sample moves toward equilibrium [$x_{max} = 0.867(4)$]. Above 581 °C, the cations disorder along the equilibrium pathway to $T_{max} = 982$ °C [$x = 0.769(3)$]. On cooling, the ordering reverses to T_B, where the maximum equilibrium order is nearly constant to room temperature [$x = 0.895(4)$]. The solid [O'Neill and Navrotsky (1983)] and dashed (Landau) curves are thermodynamic models applied to our equilibrium data. Data from O'Neill et al. (1992; their second batch of equilibrated samples from 450 to 1050 °C) are also included for comparison.

stoichiometry of the samples resulting from different methods of synthesis.

Oxygen parameter, u

The oxygen positional parameter, u, obtained in this study is within the range of 0.251–0.259 for all 2-3 spinels (O'Neill and Navrotsky 1983; Table 1). The pathway for u on heating and cooling is similar (Fig. 5a). On heating, u is about constant, then it decreases to 581 °C, and then remains nearly constant to 982 °C. However, the inversion parameter, x, increases to a maximum value at 581 °C on heating (Fig. 4). In hercynite, FeAl₂O₄, and spinel (proper), MgAl₂O₄, similar variations were observed (Harrison et al. 1998; Redfern et al. 1999).

For the data at equilibrium, x lies along the equilibrium pathway as shown in Figure 4 as a solid line, and u is nearly constant (Fig. 5b). For non-equilibrium data, as x is constant [$x = 0.841(4)$ or $0.895(4)$; Fig. 4], the u value alone increases slightly (Fig. 5b). For magnesioferrite (O'Neill et al. 1992) and other spinels (e.g., Harrison et al. 1998; Redfern et al. 1999; Andreozzi et al. 2000; Andreozzi and Princivalle 2002; Carbonin et al. 2002) a linear relationship exists between u and x, but such correlation was not observed in this study. Levy et al. (2004) also observe the non-linearity between u and x in magnesioferrite.

Bond distances

On cooling and heating, the l_{tet-O} distances have similar values. On heating, the l_{tet-O} seems to increase, then decrease to 581 °C, and increase slightly to 982 °C (Fig. 6a). The l_{tet-O} distance is obtained from the following equation: $l_{tet-O} = a (u - 1/8) \sqrt{3}$. The pathway on heating and cooling is similar as the l_{oct-O} distance varies smoothly with temperature (Fig. 6b). The l_{oct-O}

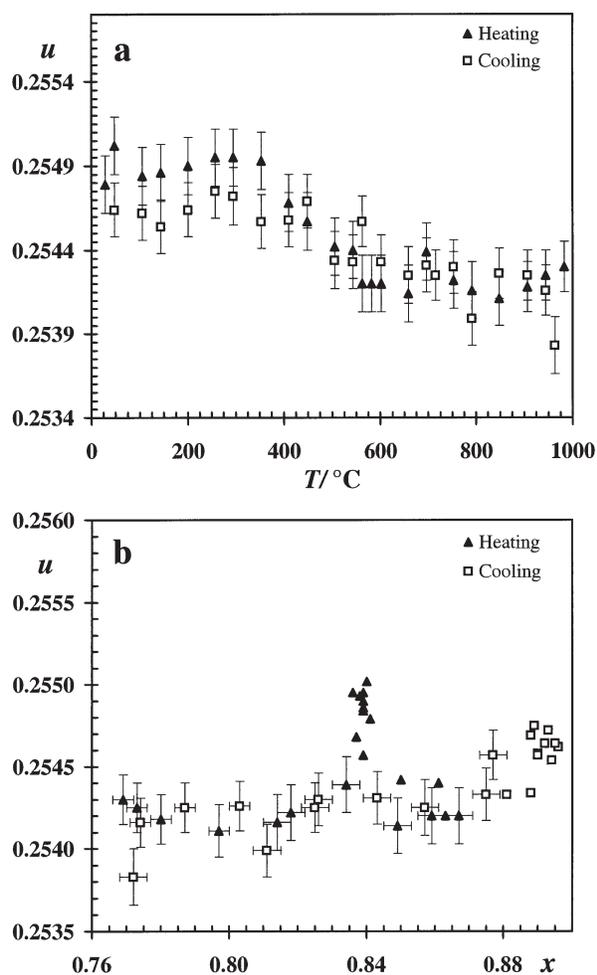**FIGURE 5.** The variation of u (**a**) with temperature and (**b**) with x. Error bars for all the data points are similar to those shown, but some error bars are excluded for clarity

distance is obtained from the following equation (O'Neill and Navrotsky 1983): $l_{oct-O} = a (3u^2 - 2u + 3/8)^{1/2}$. The octahedral site affects the cell parameter more than the tetrahedral site as l_{tet-O} is nearly constant (Figs. 6a and 6b). The $l_{tet-oct}$ and $l_{oct-oct}$ distances are related to the cell edge by the following relationships obtained from the geometry of the structure: $l_{tet-oct} = 0.41458 \, a$ Å and $l_{oct-oct} = 0.35355 \, a$ Å. The variations of x with $l_{tet-oct}$, $l_{oct-oct}$, and a are shown in Figure 7. The graphs in Figure 7 are similar to those showing the variation of x with temperature (Fig. 4).

Isotropic displacement parameters

At 28 °C, the isotropic displacement parameters, U, for the atoms increase in the following order: U(tet = tetrahedra) < U(oct = octahedra) < U(O = oxygen). The isotropic displacement parameters for the tetrahedral, octahedral, and O atom sites are different and they all increase with temperature (Fig. 8). Generally, the U parameters vary in a systematic manner. U(tet) is the smallest because of the small tetrahedral environment, while U(O) is the largest because it is the lightest atom in the structure. For any site, the U values on heating are generally higher than those on cooling at any temperature.
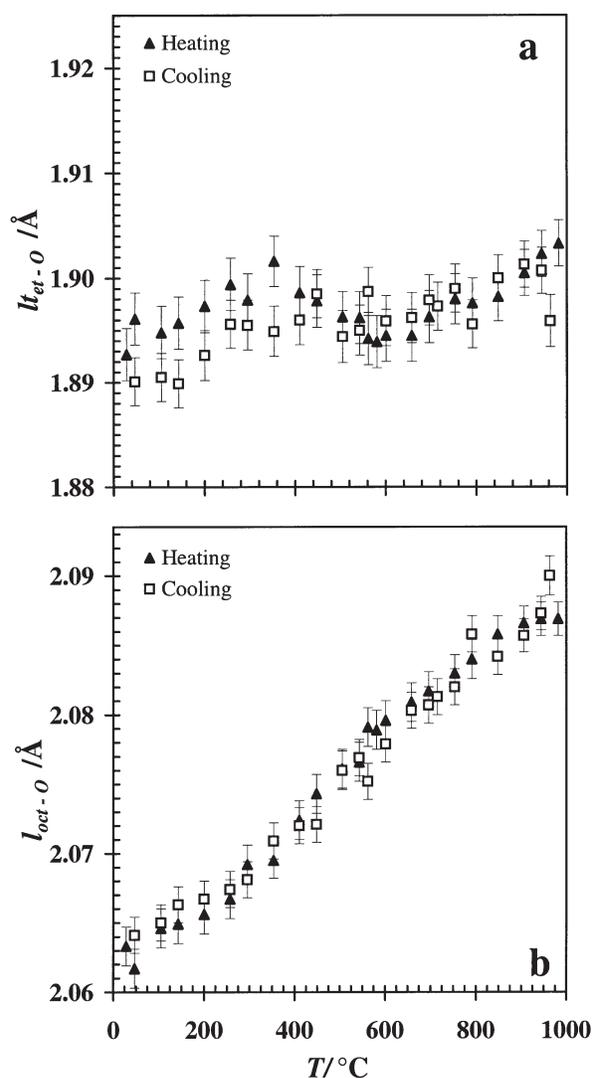

FIGURE 6. The variation of (**a**) l_{tet-O} and (**b**) l_{oct-O} with temperature. The pathway on cooling is similar to that on heating.

Thermal analyses: DSC, DDSC, and TG curves

In the first experiment, using about 15 mg of sample, the DSC curve contained an exothermic peak at about 550 °C. The energy change associated with this peak is –162 J/g (= –32 KJ/mol; Fig. 9a). In a second experiment, using about 8 mg of sample, the above exothermic peak occurred at 568 °C (Fig. 9b). The exothermic peak corresponds to the point where the cations are in a relaxed state, T_{relax}, which was also observed in the *Rietveld* refinements at about 581 °C (see Fig. 4). In the second experiment, the second and third heating cycles did not contain the exothermic peak indicating that the cation relaxation is irreversible. This is expected because the initial sample has some degree of cation order that is quenched, so during the first heating cycle, the cation distribution reaches a more relaxed state at T_{relax} (i.e., more ordered compared to the initial state). On cooling and subsequent immediate heating, the cation distribution is more relaxed, so the activation barrier that gives rise to the
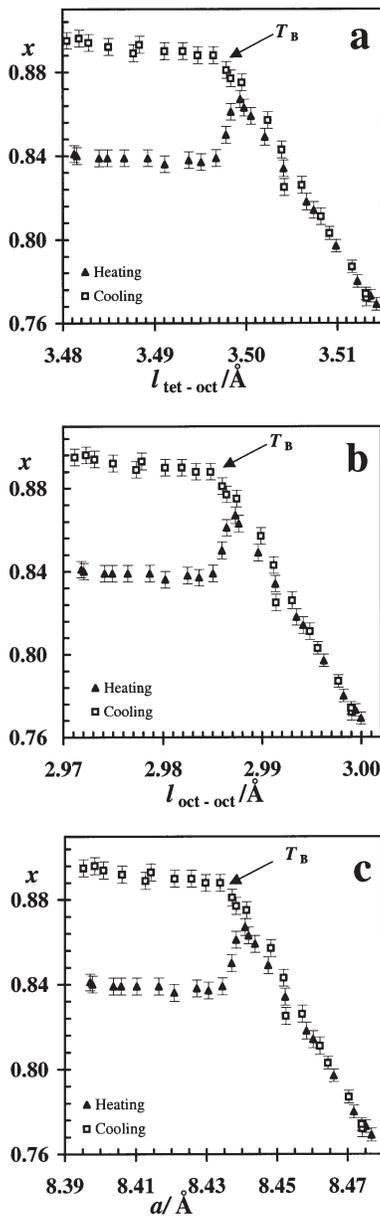
FIGURE 7. Variation of x with (**a**) $l_{tet-oct}$, (**b**) $l_{oct-oct}$, and (**c**) a. These figures are similar to Figure 4.

exothermic peak is not observed in the second and third heating cycles (Fig. 9b).

The magnetic structure of MgFe$_2$O$_4$ is that of a Néel Q-type ferrimagnet (Blasse 1964; Néel 1948). Using differential thermal analyses (DTA), Blum et al. (1957) indicated that the Curie temperature, denoted by T_{Curie}, of a magnetic material produces an endothermic peak, at about 600 °C in ferrites. Allen (1966) obtained a sharp exothermic DTA peak at 450 °C for MgFe$_2$O$_4$, which was reversible on cooling. However, in the present study, we obtain an irreversible exothermic peak at about 550 °C, and we consider this to arise from cation relaxation. The T_{Curie} for MgFe$_2$O$_4$ occurs at about 300 °C (Harrison and Putnis 1999; O'Neill et al. 1992). It does not appear that the T_{Curie} can be
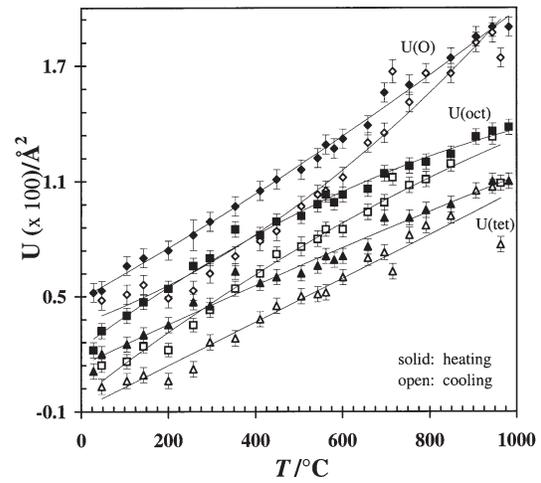

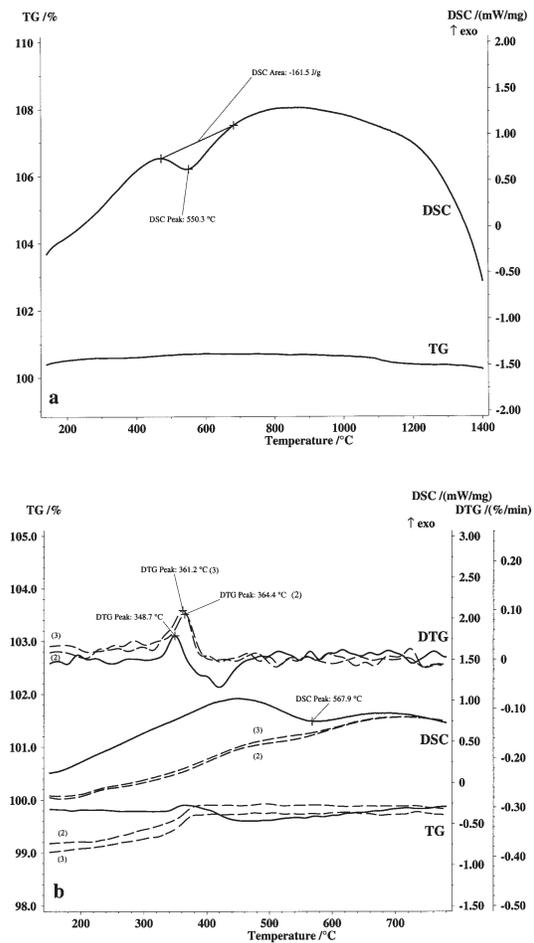**FIGURE 8.** Variation of isotropic displacement parameters with temperature.

FIGURE 9. DSC, TG, and DTG curves for MgFe$_2$O$_4$ together with characteristic data. (**a**) In the first experiment, the exothermic peak occurred at 550 °C = T_{relax} (cation relaxation temperature). (**b**) In the second experiment in a magnetic field, T_{relax} occurred at 568 °C and was not observed in the second (2) and third (3) heating cycles (dashed curves). The TG curves show changes in the effective weight of the sample at $T_{Curie} \approx 360$ °C.

clearly observed by the DSC/DTA techniques. For the second experimental run in a magnetic field, we observed changes in the effective weight of the sample at about 360 °C (= T_{Curie}) as indicated by the TG curves (Fig. 9b). The magnetic field causes this apparent change in the effective weight of the sample at T_{Curie} because of the rapid loss of spontaneous magnetization. Similar observations were also made by Walters and Wirtz (1971) and Šepelák et al. (2001).

Harrison and Putnis (1999) reported an empirical equation relating T_{Curie} of MgFe$_2$O$_4$ with the temperature of equilibration (annealing temperature = T_a) based on the data of O'Neill et al. (1992). The equation is $T_{Curie} = 489.186 - 0.296\, T_a + 0.00009875\, T_a^2$. Using this equation, T_{Curie} calculated on the basis of our synthesis temperature of 900 °C (= T_a) is 303 °C, which is in good agreement with the results of O'Neill et al. (1992; Fig. 10a), as it was obtained from the above equation. Figure 10b displays the variation of T_{Curie} with x using the data from O'Neill et al. (1992). To plot our data on this graph, we needed a value for x at 900 °C, which is our synthesis temperature. The equilibrium value for x is approximated by the value observed in situ at 906 °C [$x_{heating} = 0.780(3)$ and $x_{cooling} = 0.787(3)$; Table 1]. This value (plotted against the calculated $T_{Curie} = 303$ °C) lies close to the trend line indicated by the data of O'Neill et al. (1992; Fig. 10b). Using our x value at 906 °C, a T_{Curie} of about 315 °C was obtained from the equation in Figure 10b. Curie temperatures decrease with increasing equilibration temperatures, which leads to more disorder (Harrison and Putnis 1999; O'Neill et al. 1992; Walters and Wirtz 1971). Stoichiometry, thermal treatment, and the intracrystalline distribution of cations greatly affect T_{Curie} (Harrison and Putnis 1999).

Thermodynamic modeling

Thermodynamic models for cation ordering in spinels are available (e.g., O'Neill et al. 1992; Harrison et al. 1998; Redfern et al. 1999). The model of O'Neill and Navrotsky (1983) relates the enthalpy per formula unit of a spinel with an intermediate cation distribution, relative to the same spinel with a normal cation distribution, as a quadratic function of the degree of inversion, x:

$$\Delta H = \alpha x + \beta x^2. \tag{1}$$

Equation 1 combined with the configurational entropy of an intermediate cation distribution results in the following expression for the change in free energy relative to a normal spinel:

$$\Delta G = \alpha x + \beta x^2 + RT \sum_{i,j} N_j X_i^j \ln X_i^j \tag{2}$$

where X_i^j is the fraction of cation i at site j, and N_j is the number of j sites per formula unit. The equilibrium pathway of x is given by $\delta \Delta G/\delta x = 0$, resulting in the following expression relating x and T at equilibrium:

$$-RT \ln \{(x^2/(1-x)(2-x))\} = \alpha + 2\beta x. \tag{3}$$

The expression between the curly brackets is the equilibrium constant, K, which is obtained from the following chemical exchange reaction in MgFe$_2$O$_4$: ^{iv}[Mg^{2+}] + ^{vi}[Fe^{3+}] $\leftrightarrow$ ^{vi}[Mg^{2+}] + ^{iv}[Fe^{3+}], $K = {}^{vi}$[Mg]^{iv}[Fe]/^{iv}[Mg]^{vi}[Fe] = $[x][x]/[1-x][2-x]$ =
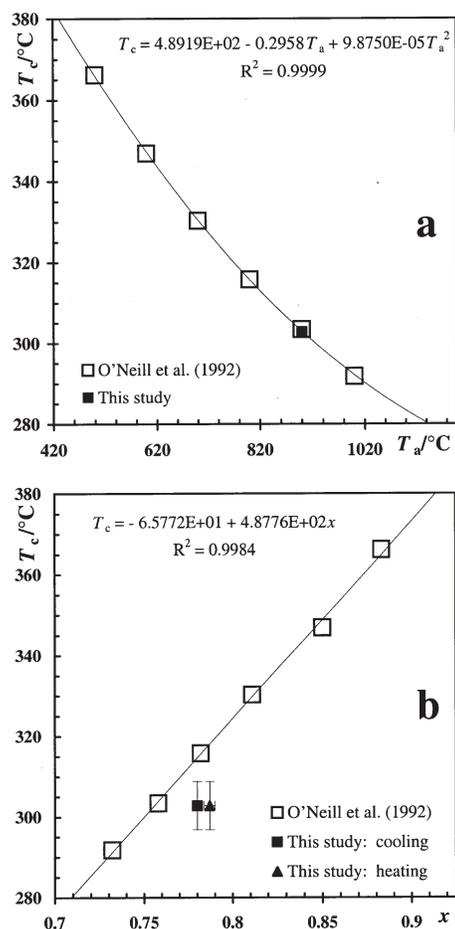

FIGURE 10. (a) Variation of T_{Curie} with T_a (annealing temperature), and **(b)** variation of T_{Curie} with x. The values of our x are the in situ values at 906 °C. Equations for O'Neill et al. (1992) data are given as inserts.

$x^2/(1-x)(2-x)$.

The equilibrium relationship (Eq. 3) describes the cation ordering behavior well for a wide range of 2–3 spinels. The α parameter ranges between +17 to +50 kJ/mol, and the β parameter ranges from –15 to –25 kJ/mol (e.g., O'Neill et al. 1991, 1992; Nell et al. 1989; O'Neill 1992, 1994; Harrison et al. 1998; Redfern et al. 1999).

The O'Neill and Navrotsky (1983) model provides a good fit to our data (solid line, Fig. 11). O'Neill et al. (1992) obtained α = +26.6 kJ/mol and β = –21.7 kJ/mol for MgFe$_2$O$_4$. A multiple non-linear least-squares fit to our equilibrium data (from about 581 to 982 °C) yielded: α = +24.8 kJ/mol and β = –21.1 kJ/mol (R^2 = 0.9907).

Another thermodynamic model for cation ordering in spinels, based on the Landau theory of phase transitions (Landau and Lifshitz 1980) was proposed by Carpenter et al. (1994) and Carpenter and Salje (1994). In Landau theory, the free energy of an intermediate spinel is calculated relative to a hypothetical spinel with a fully disordered cation distribution. Therefore, an alternative order parameter, Q, is chosen to describe the cation distribution, such that complete disorder corresponds to $Q = 0$, and
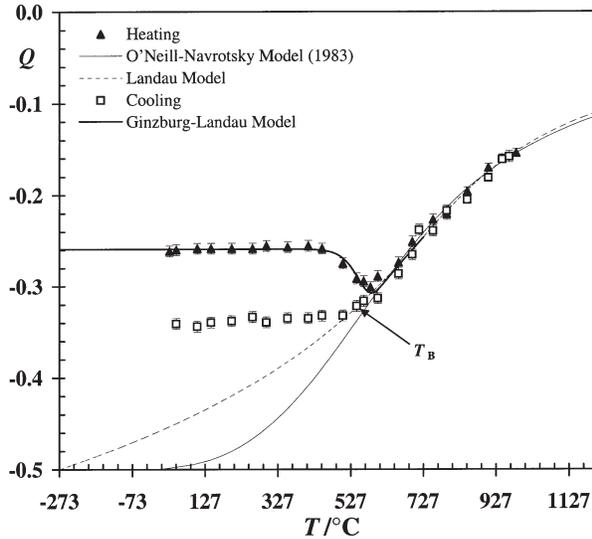
FIGURE 11. Thermodynamic models: thin solid line is a fit to our data using O'Neill and Navrotsky (1983) model, and the dashed line is the Landau fit. Thick solid line is the calculated non-equilibrium behavior using the Ginzburg-Landau rate law with the thermodynamic driving force given by the O'Neill and Navrotsky (1983) model. The thermodynamic models show that perfect order ($Q = -0.5$ in inverse spinel) occurs at -273 °C and maximum disorder ($Q = 0$) occurs at infinite temperature.

$$Q = 1 - (3/2)\,x \qquad (4)$$

where x is the inversion parameter. Accordingly, normal and inverse cation distributions have $Q = 1$ and $Q = -0.5$, respectively. The change in free energy relative to the fully disordered state at the temperature of interest is given as an expansion in terms of Q (e.g., Harrison et al. 1998):

$$\Delta G = -hQ + 1/2\ a(T - T_c)Q^2 + 1/6\ cQ^6 \qquad (5)$$

where h, a, T_c, and c are constants. The free energy in Equation 5 differs from that in Equation 2 in two respects. First, ΔH due to ordering in Equation 5 contains linear, quadratic, and 6th order terms, whereas ΔH in Equation 2 contains linear and quadratic terms. Secondly, the entropy change due to ordering in Equation 2 is the exact form of the configurational entropy, while in Equation 5 it is a simple quadratic function of the order parameter.

Setting $\delta\Delta G/\delta Q = 0$ in Equation 5 and applying the constraint that $Q = -0.5$ at 0 K for inverse spinel results in an expression relating Q and T at equilibrium:

$$T = T_c + [0.5T_c\ (1 - c'Q^5)]/(c'0.5^5 + 1)Q \qquad (6)$$

where c' $= c/h$ (Harrison and Putnis 1997).

A least-squares fit to our equilibrium data (from about 581 to 982 °C) yielded $T_c = 705$ K and c' $= -165$ ($R^2 = 0.9919$). The result of the fit is shown as the dashed line in Figure 11. Both the O'Neill and Navrotsky (1983) and Landau models fit our data quite well. However, these models cannot be extrapolated beyond the experimental range because they diverge at low temperatures.

In comparison, Harrison and Putnis (1997) obtained $T_c = 790$ K and c' $= -295$ for MgFe$_2$O$_4$ after fitting the data from O'Neill et al. (1992). Both the O'Neill and Navrotsky (1983) and Landau models approach perfect order ($Q = -0.5$ for inverse spinel) at 0 K, and by definition of non-convergent ordering, they never go to maximum disorder ($Q = 0$) at any finite temperature (Fig. 11). O'Neill and Navrotsky (1983) and Landau thermodynamic models describe the equilibrium ordering process quite well for our MgFe$_2$O$_4$ sample.

Ginzburg-Landau rate law: Kinetic behavior

Harrison and Putnis (1996) and Redfern et al. (1996) apply the Ginzburg-Landau rate law (Carpenter and Salje 1989; Salje 1988) to quantify cation relaxation, which occurs when materials are heated slowly to high temperatures. The Ginzburg-Landau rate law is described by the following relationship:

$$dQ/dt = -(\gamma/2RT)\exp(-\Delta H^*/RT)\delta\Delta G/\delta Q \qquad (7)$$

where t is time, γ is a frequency factor, $-\Delta H^*$ is the activation energy, and ΔG is the free energy potential describing cation ordering.

To apply the O'Neill and Navrotsky (1983) model to the Ginzburg-Landau rate law, the free energy of ordering was recast in terms of Q, using the symmetric formalism of Holland and Powell (1996). The heating rate used in the calculations was 600 K/h, which was the same as that used for our data collection process. The frequency factor, $\gamma = 1.354 \times 10^9$ s^{-1}, was used (Harrison 1997). The activation energy was chosen in order to fit the experimental data and a value of 186 KJ/mol gave the best fit. Both the activation energy and Q were allowed to vary in the kinetic calculations beginning from 25 °C (Fig. 11).

The cation ordering behavior in MgFe$_2$O$_4$ is similar to that for MgAl$_2$O$_4$ and FeAl$_2$O$_4$ (Redfern et al. 1999; Harrison et al. 1998). The Ginzburg-Landau rate law (Carpenter and Salje 1989; Salje 1988) and the O'Neill and Navrotsky (1983) kinetic driving force provide an excellent description of the relaxation process in these samples. In MgFe$_2$O$_4$ the system rapidly approaches the equilibrium curve between 505 and 581 °C. This occurs because the kinetics of ordering becomes fast enough to allow x or Q to change on the time scale of the experiment at these temperatures. As the temperature is raised slightly over 581 °C, the calculated heating curve oversteps the equilibrium curve (Fig. 11) because $dQ/dt = 0$ when $\delta\Delta G/\delta Q = 0$ (Eq. 7; Harrison et al. 1998). Harrison et al. (1998) obtained a negligible overstep with their heating rate of 50 K/hr. The faster rate in this study also gave a negligible overstep (heating rate = 600 K/h). The overstep size can be more significant at faster heating rates (Harrison and Putnis 1996).

We determined the cation ordering in magnesioferrite using in situ synchrotron X-ray powder-diffraction data that are better than data obtained from quenched samples because the structure at high temperature is unquenchable. At 581 °C, a discontinuity was observed in the a cell parameter that corresponds to relaxation of the cation distribution. DSC analyses also gave a similar relaxation temperature ($T_{relax} = 550$ °C). The T_{Curie} was obtained from TG analyses ($T_{Curie} \approx 360$ °C) for experiments carried out in a magnetic field. Significant cation disorder occurs in the inverse

spinel, MgFe$_2$O$_4$, up to 982 °C, which is comparable to other normal spinels (hercynite and spinel proper). Thermodynamic models fit the data in our study quite well.

ACKNOWLEDGMENTS

REFERENCES CITED

Allen, W.C. (1966) Temperature dependence of properties of magnesium ferrite. Journal of the American Ceramic Society, 49, 257–260.

Andreozzi, G.B. and Princivalle, F. (2002) Kinetics of cation ordering in synthetic MgAl$_2$O$_4$ spinel. American Mineralogist, 87, 838–844.

Andreozzi, G.B., Princivalle, F., Skogby, H., and Giusta, A.D. (2000) Cation ordering and structural variations with temperature in MgAl$_2$O$_4$ spinel: an X-ray single-crystal study. American Mineralogist, 85, 1164–1171.

Bacon, G.E. and Roberts, F.F. (1953) Neutron diffraction studies of magnesium ferrite-aluminate powders. Acta Crystallogrphica, 6, 57–62.

Blasse, G. (1964) Crystal chemistry and some magnetic properties of mixed metal oxides with spinel structure. Philips Research Reports Supplements, 3, 1–139.

Blum, S.L., Paladino, A.E., and Rubin, L.G. (1957) Differential thermal analysis technique for determining Curie points. American Ceramic Society Bulletin, 36, 175–76.

Carbonin, S., Martignago, F., Menegazzo, G., and Dal Negro, A. (2002) X-ray single crystal study of spinels: in situ heating. Physics and Chemistry of Minerals, 29, 503–514.

Carpenter, M.A. and Salje, E.K.H. (1989) Time-dependent Landau theory for order/disorder processes in minerals. Mineralogical Magazine, 53, 483–504.

——— (1994) Thermodynamics of nonconvergent cation ordering in minerals: II. Spinels and the orthopyroxene solid solution. American Mineralogist, 79, 1068–1083.

Carpenter, M.A., Powell, R.A., and Salje, E.K.H. (1994) Thermodynamics of nonconvergent cation ordering in minerals: I. An alternative approach. American Mineralogist, 79, 1053–1067.

Faller, J.G. and Birchenall, C.E. (1970) The temperature dependence of ordering in magnesium ferrite. Journal of Applied Crystallography, 3, 496–503.

Hammersley, J. (1996) Fit2d user manual. ESRF publication, Grenoble, France.

Harrison, R.J. (1997) Magnetic properties of the magnetite-spinel solid solution. Ph. D. thesis, University of Cambridge, U.K.

Harrison, R.J. and Putnis, A (1996) Magnetic properties of the magnetite-spinel solid solution: Curie temperatures, magnetic susceptibilities, and cation ordering. American Mineralogist, 81, 375–384.

——— (1997) The coupling between magnetic and cation ordering: A macroscopic approach. European Journal of Mineralogy, 9, 1115–1130.

——— (1999) Determination of the mechanism of cation ordering in magnesioferrite (MgFe$_2$O$_4$) from time- and temperature-dependence of magnetic susceptibility. Physics and Chemistry of Minerals, 26, 322–332.

Harrison, R.J., Redfern, S.A.T., and O'Neill, H.St.C. (1998) The temperature dependence of cation distribution in synthetic hercynite (FeAl$_2$O$_4$) from in situ neutron structure refinements. American Mineralogist, 83, 1092–1099.

Hazen, R.M. and Navrotsky, A. (1996) Effects of pressure on order-disorder reactions. American Mineralogist, 81, 1021–1035.

Henderson, C.M.B., Knight, K.S., Redfern, S.A.T, and Wood, B.J. (1996) High-temperature study of octahedral cation exchange in olivine by neutron powder diffraction. Science, 271, 1713–1715.

Holland, T. and Powell, R. (1996) Thermodynamics of order-disorder in minerals: 1. Symmetric formalism applied to minerals of fixed composition. American Mineralogist, 81, 1413–1424.

Larson, A.C. and Von Dreele, R.B. (2000) General Structure Analysis System (GSAS). Los Alamos National Laboratory Report, LAUR 86–748.

Landau, L.D. and Lifshitz, E.M. (1980) Statistical Physics, 544p. Pergamon Press, Oxford, New York.

Levy, D., Diella, V., Dapiaggi, M., Sani, A., Gemmi, M., and Pavese, A. (2004) Equation of state, structural behaviour and phase diagram of synthetic MgFe$_2$O$_4$, as a function of pressure and temperature. Physics and Chemistry of Minerals, 31, 122–129.

Merrill, R.B. and Wyllie, P.J. (1973) Absorption of iron by platinum capsules in high-pressure rock melting experiments. American Mineralogist, 58, 16–20.

Mozzi, R.L. and Paladino, A.E. (1963) Cation distributions in nonstoichiometric magnesium ferrite. Journal of Chemical Physics, 39, 435–439.

Neel, L. (1948) Propriétés magnetiques des ferrites; ferrimagnétisme et antiferromagnétisme. Annals of Physics, 3, 137–198.

Nell, J., Wood, B.J., and Mason, T.O. (1989) High temperature cation distribution in Fe$_3$O$_4$-MgFe$_2$O$_4$-FeAl$_2$O$_4$-MgAl$_2$O$_4$ spinels from thermopower and conductivity measurements. American Mineralogist, 74, 339–351.

O'Neill, H.St.C. (1992) Temperature dependence of the cation distribution in zinc ferrite (ZnFe$_2$O$_4$) from powder XRD structural refinements. European Journal of Mineralogy, 4, 571–580.

——— (1994) Temperature dependence of the cation distribution in CoAl$_2$O$_4$ spinel. European Journal of Mineralogy, 6, 603–609.

O'Neill, H.St.C. and Navrotsky, A. (1983) Simple spinels: crystallographic parameters, cation radii, lattice energies, and cation distribution. American Mineralogist, 68, 181–194.

O'Neill, H.St.C. and Wall, V.J. (1987) The olivine-orthopyroxene oxygen geobarometer, the nickel precipitation curve, and the oxygen fugacity of the Earth's upper mantle. Journal of Petrology, 28, 1169–1191.

O'Neill, H.St.C., Dollase, W.A., and Ross, C.R. (1991) Temperature dependence of the cation distribution in nickel aluminate (NiAl$_2$O$_4$) spinel: a powder XRD study. Physics and Chemistry of Minerals, 18, 302–319.

O'Neill, H.St.C., Annersten, H., and Virgo, D. (1992) The temperature dependence of the cation distribution in magnesioferrite (MgFe$_2$O$_4$) from powder XRD structural refinements and Mössbauer spectroscopy. American Mineralogist, 77, 725–740.

O'Neill, H.St.C., Redfern, S.A.T, Kesson, S., and Short, S. (2003) An in situ neutron diffraction study of cation disordering in synthetic qandilite Mg$_2$TiO$_4$ at high temperatures. American Mineralogist, 88, 860–865.

Paladino, A.E. (1960) Phase equilibria in the ferrite region of the system FeO-MgO-Fe$_2$O$_3$. Journal of the American Ceramic Society, 43, 183–191.

Redfern, S.A.T., Henderson, C.M.B., Wood, B.J., Harrison, R.J., and Knight, K.S. (1996) Determination of olivine cooling rates from metal-cation ordering. Nature, 381, 407–409.

Redfern, S.A.T., Harrison, R.J., O'Neill, H.S.C., and Wood, D.R.R. (1999) Thermodynamics and kinetics of cation ordering in MgAl$_2$O$_4$ spinel up to 1600 °C from in situ neutron diffraction. American Mineralogist, 84, 299–310.

Sack, R.O. (1982) Spinels as petrogenic indicators: activity-composition relations at low pressures. Contributions to Mineralogy and Petrology, 79, 169–186.

Salje, E.K.H. (1988) Kinetic rate laws as derived from order parameter theory I: Theoretical concepts. Physics and Chemistry of Minerals, 15, 336–348.

Šepelák, V., Schultze, D., Krumeich, F., Steinike, U., and Becker, K.D. (2001) Mechanically induced cation redistribution in magnesium ferrite and its thermal stability. Solid State Ionics, 141–142, 677–682.

Toby, B.R. (2001) EXPGUI, a graphical user interface for GSAS. Journal of Applied Crystallography, 34, 210–221.

Walters, D.S. and Wirtz, G.P. (1971) Kinetics of cation ordering in magnesium ferrite. Journal of the American Ceramic Society, 54, 563–565.